Int. J. Electrochem. Sci., 17 **(2022)** Article Number: 220834, doi: 10.20964/2022.08.17

International Journal of
ELECTROCHEMICAL
SCIENCE
www.electrochemsci.org

High-efficiency Electrochemical Dechlorination Using an Atomically Dispersed Co Catalyst in an Aqueous Phase

*Zhechuan Mao**, *Yinghua Xu*, *Ruifeng Qu*, *Xiaoyong Zhang*, *Zeqing Yao*

State Key Laboratory Breeding Base of Green Chemistry-Synthesis Technology, College of Chemical Engineering, Zhejiang University of Technology, Hangzhou 310014, China
*E-mail: 1111901023@zjut.edu.cn

Received: 1 May 2022 / *Accepted:* 30 May 2022 / *Published:* 4 July 2022

Electrochemical hydrodechlorination is a promising method for the degradation of disinfection by-products (DBPs) under mild conditions. In this study, we synthesized atomically dispersed Co on N-doped graphene (A-Co-NG) as an efficient electrocatalyst and studied its hydrodechlorination activity and reaction mechanism using trichloroacetic acid (TCAA) as a model DBP. The galvanostatic electrolysis experiments showed that the A-Co-NG catalyst had a higher dechlorination activity than that of commercial Pd/C. Using A-Co-NG, chloroacetic acids (CAAs) were completely dechlorinated to acetic acid at pH values of 3, 7, and 11. The dechlorination of CAAs by A-Co-NG follows a direct dechlorination mechanism. The first electron transfer (ET) and C-Cl bond breaking processes proceed sequentially, and the first ET step is the rate-determining step for the dechlorination of TCAA.

Keywords: Electrochemical hydrodechlorination; Single atom catalyst; Catalytic mechanism; Disinfection by-products

1. INTRODUCTION

Disinfection by-products (DBPs) are often formed during the chlorination or ozone disinfection of drinking water. These by-products are potentially harmful to human health; for example, they increase the risk of cardiovascular diseases [1,2], affect fetal growth [3], and are carcinogenic [4]. Trichloroacetic acid (TCAA), which is the most abundant DBP and has been proven to be carcinogenic, often exists in chlorinated water. The concentration limit for TCAA in drinking water is 0.1 mg/L [5,6]. At present, several technologies have been developed and applied for the dechlorination and degradation of chloroacetic acids (CAAs) [7-14]. Electrocatalytic reductive dechlorination has received significant research attention for the removal of CAAs because it can proceed at atmospheric pressure and room temperature, does not involve the use of H_2 (which is explosive), and does not cause secondary pollution.

Electrocatalyst or catalytic electrode will influence the efficiency of electrocatalytic reduction dechlorination process to a great extent [15-17]. In particular, Ag and Pd have shown high electrochemical dechlorination activities. At present, numerous types of Ag and Pd electrocatalysts (or electrodes) have been applied for the electrochemical dechlorination of CAAs [5, 18-21]. For example, using a rough Ag mesh electrode for the dechlorination of TCAA in a 0.5 M NaOH aqueous solution affords an acetic acid (AA) yield of 99% and a current efficiency (CE) of 70% [18]. Liu et al. [5] prepared a $PdIn/Al_2O_3$ catalyst for the electrochemical dechlorination of TCAA. With a current density of 0.9 mA/cm^2, 94% of the TCAA was successfully degraded within 30 min. However, Ag and Pd are precious metals, and their practical application is limited by their high costs. Therefore, various materials without precious metals have been prepared as electrocatalysts for the electrochemical dechlorination of CAAs [22-28]. Yao et al. [25] prepared amorphous Ni_2P (ANP) with a micro nanorod array in situ on a Ni foam (NF) and used it as a binderless cathode for the removal of TCAA. The dechlorination performance of the as-prepared cathode was better than that of other metal cathodes (e.g., bare NF and Pd/C). Huang et al. [27] prepared a Co-doped MoS_2 catalyst, with which TCAA could be transformed into AA in one step, without the generation of intermediate reductive dechlorination products (dichloroacetic acid (DCAA) and monochloroacetic acid (MCAA)). This exemplified that doping with Co or Ni can significantly improve the dechlorination performance. Mao et al. [28] prepared a graphene-modified Cu foam catalyst electrode and used TCAA to study its dechlorination activity. Inconveniently, large amounts of DCAA and MCAA were produced during the reaction. Although many non-noble-metal catalysts have been developed, their electrocatalytic dechlorination activities are far from the requirements.

In recent years, single-atom electrocatalysts (SAECs) have been widely used for the reduction reactions (RRs) of CO_2 (CO_2RR) [29-31], N_2 (NRR) [32,33], and O_2 (ORR) [34,35]; evolution reactions of hydrogen (HER) [36,37] and oxygen (OER) [38,39]; and electrooxidation of ethanol [40]. The reason is that their atomic utilization ratios are 100%, as well as their high activities and selectivities. SAECs also act as bridges between homogeneous and heterogeneous catalytic reactions. SAECs containing Ni and Co have shown excellent electrochemical reduction performance [41-43]; however, to our knowledge, there are no studies on Co SAECs applied to electrochemical reductive dechlorination reactions. In this study, we synthesized an electrocatalyst consisting of atomically dispersed Co on N-doped graphene (A-Co-NG) and studied its catalytic activity for the electrochemical reductive dechlorination of CAAs. The results show that A-Co-NG has a higher catalytic activity than the most advanced state-of-the-art Pd/C electrocatalyst, and that its turnover frequency (TOF, 2.3 min^{-1}) is approximately 10,000 times that of Co-MoS_2 (1.5×10^{-4} min^{-1}) [27]. In addition, the dechlorination pathway and catalytic mechanism of A-Co-NG have been revealed using cyclic voltammetry (CV) experiments.

2. EXPERIMENTAL

2.1. Chemicals

Cobalt (II) acetate tetrahydrate (99 wt.%), melamine (99 wt.%), L-alanine (99 wt.%), and a Nafion 117 solution (~5 wt.%) were purchased from Sigma-Aldrich. TCAA (99.0 wt.%), DCAA (99.0

wt.%), AA (99.0 wt.%), monopotassium phosphate, dipotassium phosphate, sodium chloride, phosphoric acid with a purity of ~85 wt.% in H_2O, and Pd on active carbon (Pd/C) with a Pd loading of 10 wt.% were purchased from Adamas-beta Co., Ltd. MCAA (99.0 wt.%) was obtained from Alfa Aesar (China) Chemical Co., Ltd. Carbon paper (CP, AvCarb P75T) was purchased from Hangzhou Saiao Technology Co. Ltd. Deionized water with a resistivity of 18 MΩ·cm was obtained from a Millipore Milli-Q system and used to prepare all solutions.

2.2. Synthesis and characterization

A-Co-NG and blank N-doped graphene (NG) were synthesized using the methods described in detail in our previous paper [44, 45]. X-ray diffraction (XRD, Thermo ARL SCINTAG X'TRA, 45 kV and 40 mA, Cu Kα), sub-ångström-resolution high-angle annular dark-field scanning transmission electron microscopy (HAADF-STEM, JEOL JEM ARM200F STEM/TEM), and transmission electron microscopy (TEM, Tecnai G2 F30 S-Twin) coupled with energy dispersive X-ray spectroscopy (EDX, Thermo NORAN VANSTAGE ESI, Thermo Fisher Scientific) were used to study the structure and morphology of the prepared catalysts. X-ray photoelectron spectroscopy (XPS, KRATOS AXIS ULTRA DLD) was used to study the surface valence states.

2.3. Dechlorination studies

The constant-current (CC) electrolysis experiments were performed in an H-type electrolytic cell separated by a Nafion-117 membrane. The reaction system was composed of a CP electrode (CP, 2 × 2 cm) modified with Pd/C, NG, or A-Co-NG, Pt sheet electrode (2 × 2 cm), and Ag/AgCl reference electrode. The cathode solution was the reaction solution (30 ml), and the anode solution was a 0.1 M phosphate buffer aqueous solution (PBS, pH = 3). During electrolysis, the cathode solution was continuously stirred. Cyclic voltammetry (CV) experiments were performed in a three-electrode system composed of a glassy carbon (GC) electrode modified with A-Co-NG (A-Co-NG/GC), Pt sheet (1 × 1 cm) auxiliary electrode, and Ag/AgCl reference electrode. All the CC and CV experiments were performed using an electrochemical workstation (CHI 660C, CH Instruments, Inc.).

The TOF was calculated using Eq. (1).

$$\mathrm{TOF}=\frac{\mathrm{N_{CAAs}}\times\alpha}{\mathrm{N}\times\mathrm{t}}, \qquad (1)$$

where N_{CAAs} is the initial number of CAAs molecules, α is the conversion of CAAs at the time t, N is the number of active metal atoms, and t is the reaction time (min) at which the reactant concentration has decreased by 50%.

2.4. Analytical methods

The concentrations of TCAA, DCAA, MCAA, AA, and Cl^- were determined via ion chromatography (IC, Dionex ICS-2100, Thermo Fischer) using standard calibration curves and a Dionex

IonPac AS11-HC column (Thermo Fischer). The precision of the mass balance in the measurement was of approximately ±3%.

2.5. Preparation of electrodes

The A-Co-NG/GC electrode was prepared by drop-casting 10 μL of a catalyst ink onto a GC electrode (3 mm in diameter), which yielded a catalyst loading of 0.708 mg/cm^2. The catalyst ink was prepared by introducing 0.05 mg of catalyst and 25 μL of 5 wt.% Nafion 117 solution into 1 ml of a 1:1 ethanol/isopropanol solution. A similar method was used to prepare a NG/GC (0.708 mg/cm^2) electrode.

The A-Co-NG-modified CP (A-Co-NG/CP) electrode was prepared by painting 10 mL of a catalyst ink onto the two surfaces of a CP electrode (2 × 2 cm), which yielded a catalyst loading of 1.25 mg/cm^2. The catalyst ink was prepared by introducing 5 mg of the catalyst into 20 mL of a 3:1 ethanol/isopropanol solution followed by sonication for 3 h. Before the catalyst ink was prepared, the catalyst was ground for 5 min using an agate mortar. A similar method was used to prepare the NG/CP and Pd/C/CP electrodes (both with catalyst loadings of 1.25 mg/cm^2).

3. RESULTS AND DISCUSSION

3.1. Characterization of A-Co-NG

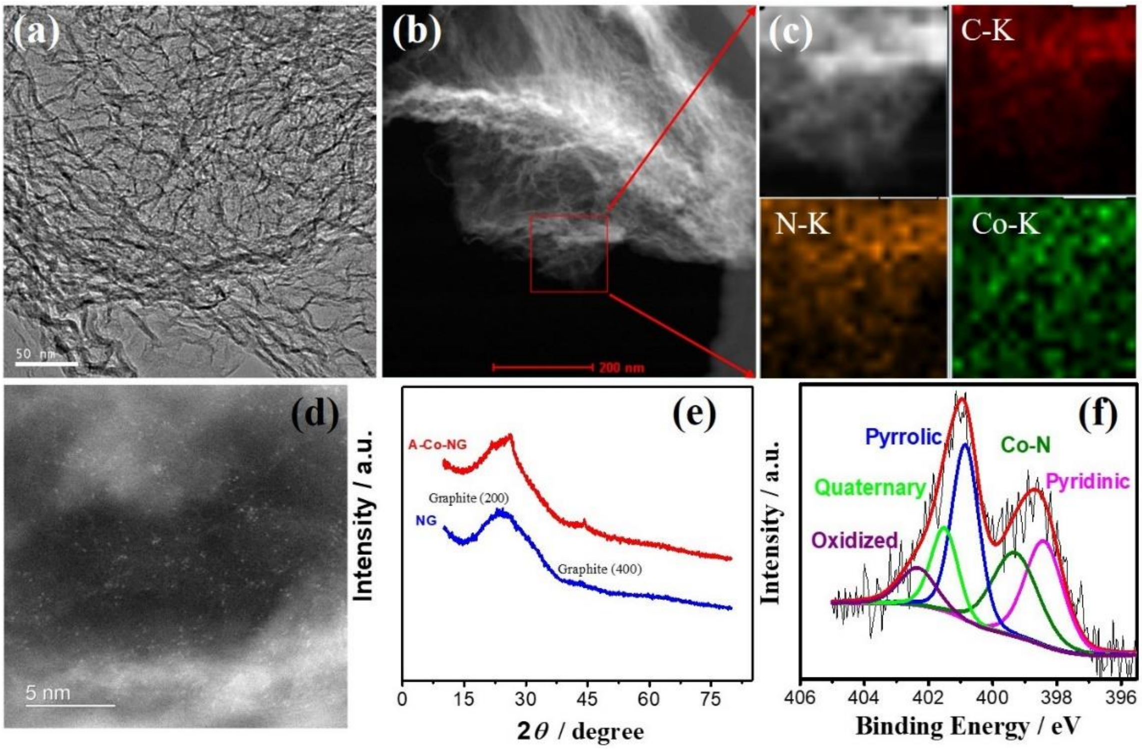

Figure 1. Structural characterization of the A-Co-NG catalyst. (a) Bright-field and (b) dark-field TEM images; (c) elemental mapping (EDX) of C, N, and Co in A-Co-NG; (d) HAADF-STEM image of A-Co-NG; (e) XRD patterns of A-Co-NG and NG catalysts; (f) high-resolution XPS spectrum of N 1s in A-Co-NG, which is deconvoluted into five Voigt-type line-shaped peaks using the Shirley background.

The prepared A-Co-NG had a two-dimensional folded surface. No Co nanoclusters or metallic Co particles were observed (Fig. 1a). The TEM dark-field image and its corresponding mapping diagram (Figs. 1b, c) show a uniform distribution of C, N, and Co atoms on the folded surface. The HAADF-STEM image (Fig. 1d) shows high-density bright spots (0.2 nm) that can be observed over the entire carbon skeleton, indicating that Co was dispersed on the carbon carrier in the form of single atoms. The XRD spectrum of A-Co-NG (Fig. 1e) shows only a diffraction peak corresponding to graphite; the peak of metallic Co is not observed, which proves that Co was atomically dispersed. The atomic composition in A-Co-NG measured using XPS was 0.77 at.% Co, 5.38 at.% N, 7.78 at.% O, and 86.07 at.% C (Table 1). The high-resolution XPS spectrum of N 1s can be deconvoluted into peaks at the binding energies corresponding to pyridine nitrogen (398.3 eV), Co-N (399.4 eV), pyrrole nitrogen (400.4 eV), quaternary nitrogen (401.3 eV), and oxidized nitrogen (402.9 EV). It can be deduced that the Co atoms in A-Co-NG coordinate with the N atoms, forming a stable catalyst.

Table 1. Elemental composition of the A-Co-NG catalyst determined using XPS.

Element	wt.%	at.%
O	9.73	7.78
N	5.89	5.38
C	80.82	86.07
Co	3.56	0.77

3.2. Electrochemical dechlorination performance

The pH of the cathode solution and current density applied to the electrode generally have a significant impact on the electrochemical reaction rate and reduction products of the reductive dechlorination [16, 17, 46]. We performed experiments to optimize these two parameters using A-Co-NG/CP as the cathode and TCAA as the reactant. As presented in Table 2, the distribution of products at three different pH values (entries 1–3) was relatively similar. Therefore, A-Co-NG has good adaptability to pH in the dechlorination of TCAA ; the pH of 7.2 was selected as the optimum because of its innocuity. Entries 2 and 4–6 show that the electrochemical dechlorination efficiency (selectivity of AA) first increased and then decreased with the increase of the applied current density. This is because at a low current density, the amount of charge generated by the electrode is insufficient, and at a high current density, the generated H_2 covers parts of the electrodes, reducing the number of catalytic active sites and decreasing the dechlorination rate. We compared the dechlorination activities of A-Co-NG with those of NG and commercial Pd/C using the optimum values of the current density and pH (entries 2, 7, and 8). The dechlorination activity of the NG/CP electrode (with which no AA was produced) was significantly lower than that of the A-Co-NG/CP electrode, implying that Co single atoms in A-Co-NG play a major role in the dechlorination of TCAA. Additionally, the dechlorination activity of A-Co-NG was much higher than that of the commercial Pd/C.

Table 2. Optimization of the reaction conditions with TCAA as the target reactant.

Entry	Cathodes	pH	Current density (mA/cm^2)	TCAA Conv. (%)	Selectivity (%)		
					DCAA	MCAA	AA
1[a]	A-Co-NG/CP	3.1	15	100	0.6	69.9	29.4
2[a]	A-Co-NG/CP	7.2	15	100	0.8	58.7	39.6
3[a]	A-Co-NG/CP	11.2	15	100	0.5	64.2	34.5
4[a]	A-Co-NG/CP	7.2	5	100	40.3	43.2	12.8
5[a]	A-Co-NG/CP	7.2	25	100	0.8	61.3	33.6
6[a]	A-Co-NG/CP	7.2	37.5	100	3.6	67.3	27.6
7[a]	NG/CP	7.2	15	100	20.3	77.6	0
8[b]	Pd/C/CP	7.2	15	100	13.2	74.6	10.9

Unless otherwise stated, 30 mL 0.1 M PBS containing 9.9 mM TCAA was used as the catholyte. The reaction time was 5 h, and the stirring speed was 1200 rpm.

[a] Catalyst loading: 5 mg.

[b] Pd loading: 0.5 mg, Catalyst loading: 5 mg.

3.3. Dechlorination pathway of CAAs

The dechlorination pathway of TCAA on the A-Co-NG/CP electrode was studied under the previously optimized conditions. TCAA was rapidly reduced to the main intermediate products, DCAA and MCAA, and totally dechlorinated eventually to form the final product, AA (Fig. 2a).

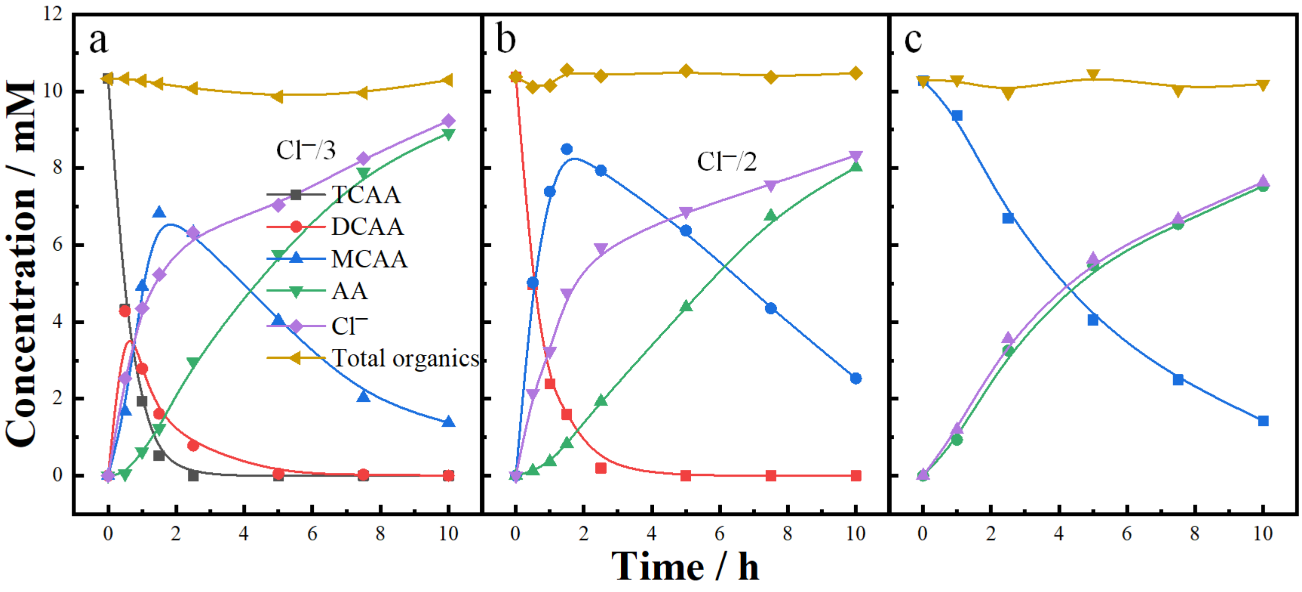

Figure 2. Concentration profiles of chloroacetic acids and their electrolytic reduction products. (a) Trichloroacetic acid (TCAA), (b) dichloroacetic acid (DCAA), and (c) monochloroacetic acid (MCAA). AA: acetic acid.

The concentrations of DCAA and MCAA increased to approximately 4.2 and 6.9 mM, respectively, and then decreased rapidly as the reaction proceeded. This phenomenon indicates that the dechlorination of TCAA might follow a step-by-step dechlorination pathway. Then, we carried out additional experiments under the same conditions using DCAA and MCAA as the starting reactants (Figs. 2b, c). With a sufficiently long reaction time, DCAA eventually transformed to AA; MCAA was the only detected intermediate (Fig. 2b). The reaction of MCAA quantitatively generated AA (Fig. 2c). These results confirm that the dechlorination process of TCAA mainly follows the TCAA → DCAA → MCAA → AA dechlorination pathway.

3.4. Dechlorination mechanism

3.4.1. Direct/indirect dechlorination

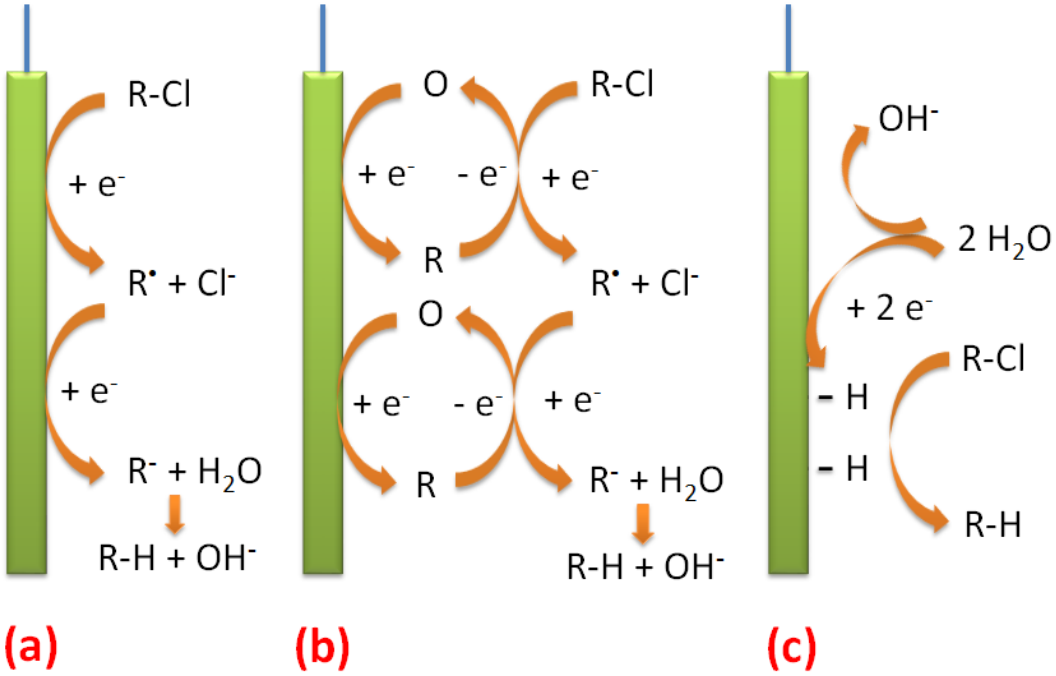

Scheme 1. Dechlorination mechanisms: (a) direct dechlorination, (b) indirect dechlorination catalyzed by a redox medium, and (c) indirect dechlorination catalyzed by adsorbed H.

The electrochemical reductive dechlorination of chlorinated organic compounds follows either a direct [18, 47, 48] or an indirect dechlorination mechanism [49-55]. In the direct mechanism, the chlorinated organic compounds directly obtain electrons from the cathode for the electroreductive dechlorination reaction (Scheme 1a). Indirect dechlorination mechanisms are mainly divided into two types. The first type involves the presence of a redox medium on the surface of the electrode or in solution, through which the electrons are transferred to the chlorinated organics (Scheme 1b). The second type is an electrocatalytic hydrogenation reduction reaction in the aqueous solution. The water molecules or hydrogen ions obtain electrons from the electrode surface and convert into adsorbed hydrogen atoms, which then react with the organic compounds adsorbed on the electrode surface to produce hydrogenation products (Scheme 1c).

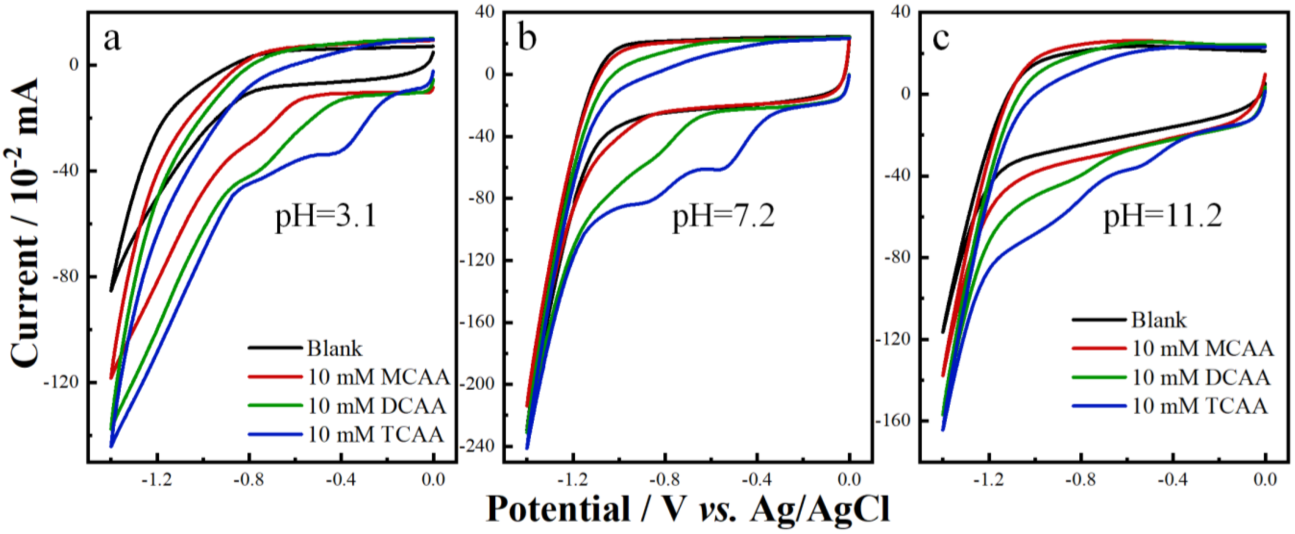

Figure 3. Cyclic voltammograms for the dechlorination of chloroacetic acids with an A-Co-NG/GC electrode in 0.1 M phosphate buffer aqueous solutions with different pH values. Scan rate (v): 0.05 V/s. Temperature: 298 K. (a) pH=3.1; (b) pH=7.2; (a) pH=11.2.

If it follows the direct dechlorination mechanism, different chlorinated substrates have different initial reduction potentials on the CV curves [18, 47, 48]; if it follows one of the indirect dechlorination mechanisms, different chlorinated substrates have practically identical initial reduction potentials on the CV curves [49-51, 54, 55], and a pair of redox peaks can be observed on the CV curve of the blank solution [49-55]. When there is no redox medium, this pair of peaks corresponds to the reduction of hydrogen ions and oxidation of adsorbed hydrogen atoms [49, 54, 55]. By contrast, when there is a redox medium, the pair of peaks corresponds to the redox process of the medium [50-53]. The reduction peak current will increase as the chlorinated organic substrates are added, and the oxidation peak current will decrease [49-55]. Therefore, we can evaluate the dechlorination mechanism of a specific reaction using the CV curves. Fig. 3 shows that under different pH conditions, the CV curves of MCAA, DCAA, and TCAA have different initial reduction potentials, and no redox peaks similar to the aforementioned peaks are visible in the blank solution for any value of pH. These results demonstrate that the reductive dechlorination process of MCAA, DCAA, and TCAA on the A-Co-NG/GC electrode follows the direct dechlorination mechanism.

To further prove that the electrochemical dechlorination of CAAs on the A-Co-NG catalyst follows a direct dechlorination mechanism, we performed catalytic hydrogenation experiments (Table 3). At a pH of 7.2, hydrogen was introduced into the cathode liquid as a reducing agent. After 5 h of hydrogen injection, the concentrations of TCAA, DCAA, and MCAA showed no changes. This indicates that the A-Co-NG/CP catalytic electrode cannot dissociate and adsorb hydrogen or that the generated hydrogen atoms cannot react with the CAAs. In addition, the CV curves show that the second reduction potential of TCAA is consistent with the first one of DCAA, and the third reduction potential of TCAA is consistent with the second one of DCAA and that of MCAA. Therefore, the electrochemical dechlorination of CAAs on the A-Co-NG/CP electrode follows a gradual dechlorination pathway for all values of pH. The reaction activity followed the order of TCAA > DCAA > MCAA.

Table 3. Catalytic hydrodechlorination of chloroacetic acids (10 mM) in 30 mL 0.1 M PBS (pH = 7) using H_2 (30 sccm) as reductant. Reaction time: 5 h.

Entry	Reactant	Catalyst	Atmosphere	Conv. (%)
1	TCAA	5 mg A-Co-NG	H_2	0
2	DCAA	5 mg A-Co-NG	H_2	0
3	MCAA	5 mg A-Co-NG	H_2	0

3.4.2. Mechanistic origin of the catalytic activity and electron transfer (ET) mechanisms

The direct electrochemical reduction dechlorination is described using Eqs. 2–6 [56-58]. The first ET reactions can gradually form free radical anions ($RCl^{\bullet-}$, stepwise mechanism, Eqs. 2 and 3) or destroy the C-Cl bonds and form free radicals ($R^{\bullet}$, synergistic mechanism, Eq. 4).

$$R\text{-}Cl + e^- \leftrightarrow RCl^{\bullet-} \qquad (E^{\Theta}_{1\text{-}1}) \qquad (2)$$

$$RCl^{\bullet-} \rightarrow R^{\bullet} + Cl^- \qquad (3)$$

$$R\text{-}Cl + e^- \rightarrow R^{\bullet} + Cl^- \qquad (E^{\Theta}_{1\text{-}2}) \qquad (4)$$

$$R^{\bullet} + e^- \leftrightarrow R^- \qquad (E^{\Theta}_{2}) \qquad (5)$$

$$R^- + H_2O \rightarrow RH + OH^- \qquad (\text{fast}) \qquad (6)$$

The relationship between the shape of the dechlorination peaks in the CV curves and v can be analyzed to determine which of the two ET mechanisms is followed by the dechlorination reactions.

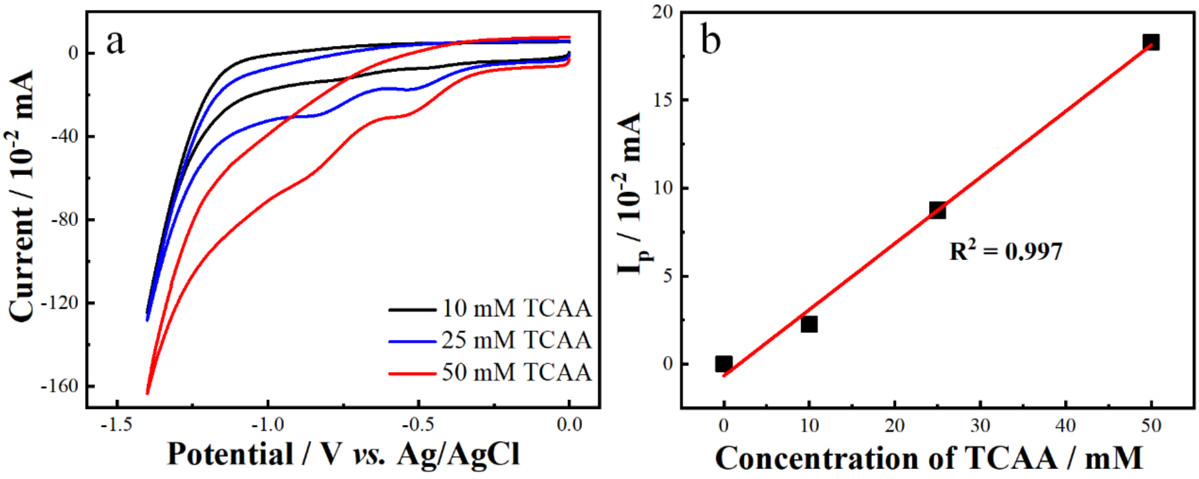

Figure 4. (a) Cyclic voltammogram of A-Co-NG/GC in a 0.1 M PBS (pH = 7) with different concentrations of TCAA. (b) Dependence of the first peak current (I_p) on the concentration of TCAA.

Therefore, we calculated the ET coefficient k (Eq. 7). Here, E_p and $E_{p/2}$ represent the peak and half-peak potentials, respectively. In the step-by-step mechanism, when the process is controlled by hybrid dynamics (i.e., the energy barriers for the ET and bond fracture are very similar) or bond fracture, the value of k is between 0.5 and 1. In contrast, if the ET is the controlling step, the standard potential and reduction potential are close, and $k \approx 0.5$.

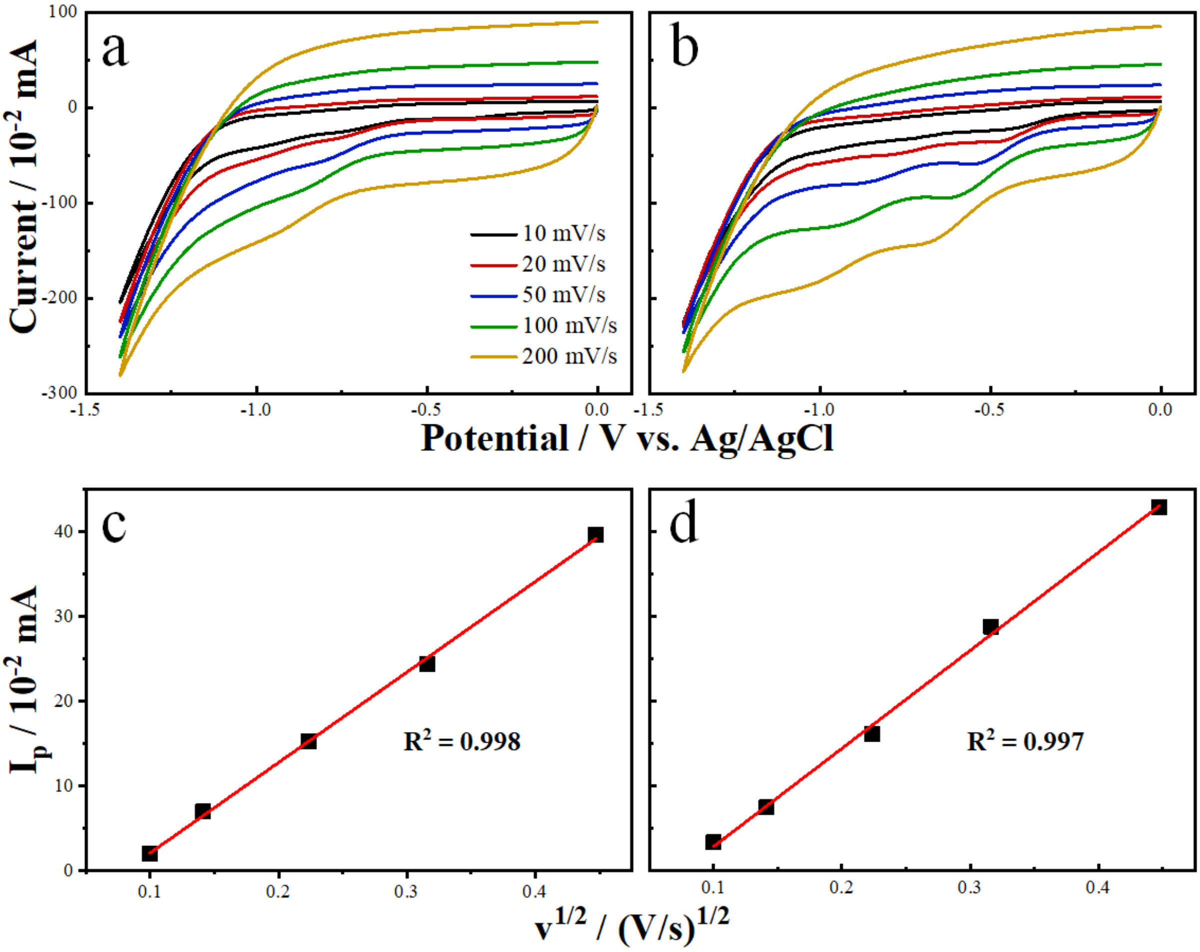

Figure 5. CV curve of A-Co-NG/GC with different v values in a 0.1 M phosphate buffer aqueous solution of pH = 7 with 10 mM of (a) DCAA and (b) TCAA. Dependence of the first I_p on $v^{1/2}$ for (c) DCAA and (d) TCAA.

In the synergistic mechanism, the reduction potential is lower than the standard potential owing to the large amount of energy released during the bond breaking, and $k < 0.5$. This method is often used to distinguish between synergistic and step-by-step mechanisms, and it is applicable to both proton and aprotic solvents. Notably, this method is only applicable to mass transfer processes controlled by diffusion.

$$k = -1.857 \times \frac{RT}{F(E_p - E_{p/2})} = \frac{0.0477}{E_p - E_{p/2}} \text{ V at } 298\,\text{K} \qquad (7)$$

where R is the gas constant (8.314J/(K·mol)), T is the temperature (K), F is the faraday constant (96500 C/mol).

Table 4. Data of the reduction peaks at different v values for the A-Co-NG/GC electrode in a 0.1 M PBS of pH = 7 with 10 mM TCAA under a N_2 atmosphere at a temperature of 298 K.

v (V/s)	E_p (V)	$E_{p/2}$ (V)	$E_{p/2} – E_p$ (V)	k^a	k_a^b
0.01	-0.44	-0.36	-0.08	0.60	0.50
0.02	-0.48	-0.40	-0.08	0.60	
0.05	-0.55	-0.45	-0.10	0.48	
0.1	-0.62	-0.51	-0.11	0.43	
0.2	-0.69	-0.57	-0.12	0.40	

[a] Calculated from Eq. 7. [b] Average value of k.

Table 5. Data of the reduction peaks at different v values for the A-Co-NG/GC disk electrode in a 0.1 M PBS of pH = 7 with 10 mM DCAA under a N_2 atmosphere at a temperature of 298 K.

v (V/s)	E_p (V)	$E_{p/2}$ (V)	$E_{p/2} – E_p$ (V)	k^a	k_a^b
0.01	-0.78	-0.66	0.12	0.40	0.33
0.02	-0.81	-0.67	0.14	0.34	
0.05	-0.84	-0.69	0.15	0.32	
0.1	-0.89	0.73	0.16	0.29	
0.2	-0.94	-0.77	0.17	0.28	

[a] Calculated from Eq. 7. [b] Average value of k.

Because there did not show any reduction peak on the CV curve of MCAA, we only measured the CV curves of DCAA and TCAA at different v values. As shown in Figs. 4 and 5, the reduction peak currents of DCAA and TCAA are directly proportional to the square root of v ($v^{1/2}$) and concentration of substrate. This implies that the step involving the diffusion of DCAA and TCAA from the bulk solution to the electrode surface dynamically limits the reductive dechlorination process.

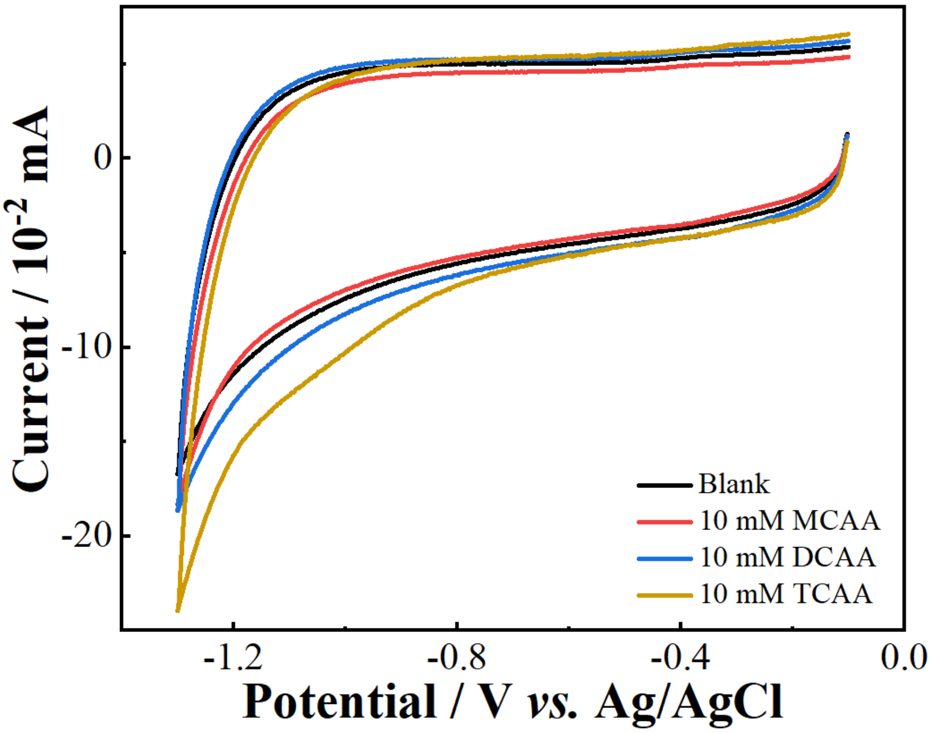

Figure 6. Cyclic voltammogram for the NG/GC electrode in a 0.1 M phosphate buffer aqueous solution of pH = 7 with 10 mM of TCAA, DCAA, or MCAA [44].

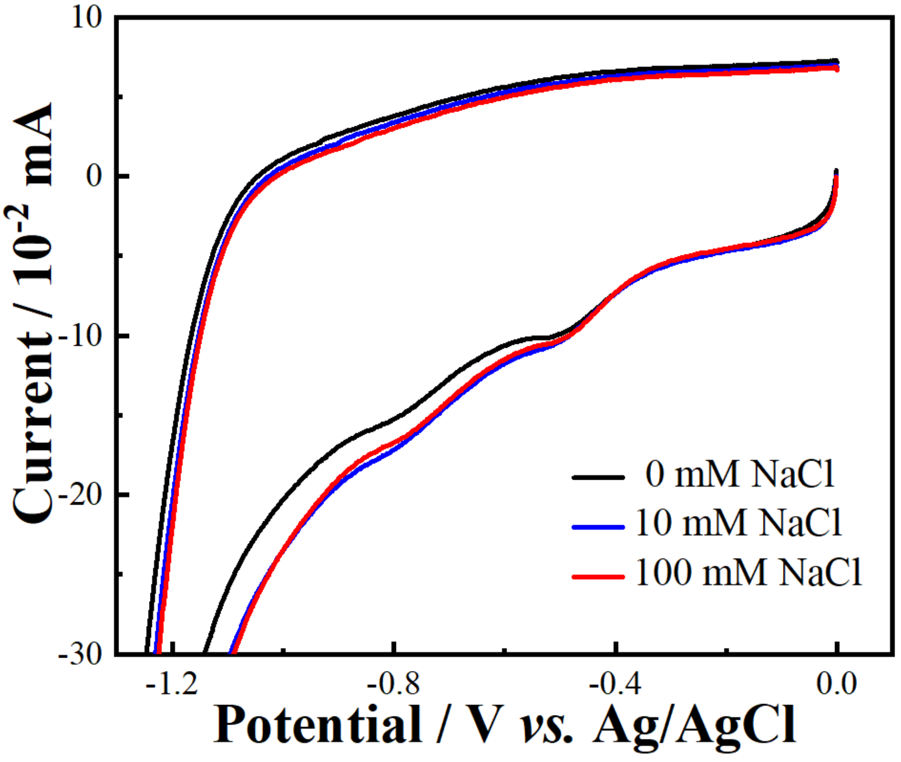

Figure 7. Cyclic voltammogram for the A-Co-NG/GC electrode in a 0.1 M phosphate buffer aqueous solution with 10 mM TCAA and different concentrations of NaCl under a N_2 atmosphere; v: 0.05 V/s; temperature: 298 K.

The CV curves of TCAA and DCAA are prone to severe deformation when the scanning rate is high (>0.2 V/s) because of the high charging capacitance of the A-Co-NG/GC electrode. Therefore, we only used low scanning rates to study the CV curves. The values of k (Tables 4 and 5) were calculated using Eq. 7. The average k (k_a) value for the dechlorination of TCAA to generate DCAA was 0.5 (Table 4), indicating that the first ET step is the rate-determining step; the reduction peak potential is close to the equilibrium potential of the first ET step. According to our previous study [44], the potential of the reduction peak of the dechlorination of TCAA to DCAA on the NG/GC electrode (Fig. 6, −0.65 V) is much lower than that on the A-Co-NG/GC electrode (Fig. 3b, −0.29 V). Therefore, it is likely that the Co on A-Co-NG catalyzes the ET step and the TCAA and generated free radical anion are adsorbed on the surface of the A-Co-NG/GC electrode. The k_a is 0.33 when DCAA is dechlorinated to form MCAA (Table 5). Therefore, this dechlorination process is likely to be controlled by the breaking of the carbon-chlorine bond; the potential of this process on the A-Co-NG/GC electrode is much higher than that on the NG/GC electrode.

The presence of Cl^- in the solution can hinder the desorption of Cl^-; therefore, this step might also be the rate-determining step. We conducted CV experiments with different concentrations of Cl^- in the solution to explore this possibility. Fig. 7 shows that the concentration of Cl^- has negligible influence on the peak types and dechlorination reduction potentials of TCAA and DCAA. Therefore, we believe that the desorption of Cl^- is not rate-determining.

3.5. Catalytic activity comparison

Table 6. Activity comparison of A-Co-NG with various reported electrocatalysts for the dechlorination of CAAs.

Catalyst	Cathode	Reactant	TOF[a] (min^{-1})	Main products[b]	Refs.
Co-MoS_2	Co-MoS_2/CF[c]	TCAA	1.5×10^{-4}	AA	[27]
Pd-Ag	Pd-Ag/Ni foam	DCAA	0.035	MCAA, AA	[59]
Ni_2P	Ni_2P/Ni foam	TCAA	9.5×10^{-5}	MCAA, AA	[25]
Pd/rGO[c]	Pd/rGO /CP	TCAA	5.8×10^{-5}	MCAA, AA	[60]
Pd-In/Al_2O_3 /RuO_2	Pd-In/Al_2O_3/RuO_2/ Ti mesh	TCAA	1.8×10^{-3}	DCAA,MCAA	[5]
A-Co-NG	A-Co-NG /CP	TCAA	2.3	AA	This work
A-Co-NG	A-Co-NG /CP	DCAA	1.8	AA	This work

[a] . TOF was calculated by Eq. (1).

[b] . The main products at the end of dechlorination reaction.

[c] . CF is carbon felt and rGO is reduced graphene oxide.

Taking electrochemical dechlorination of CAAs as the model reaction, the catalytic activity of A-Co-NG was compared with 5 typical electrocatalysts reported in recent literature [5, 25, 27, 59, 60]

(Table 6). Among which, A-Co-NG shows the highest TOF and the best selectivity, rendering A-Co-NG a very promising electrocatalyst for treatment of chlorinated DBPs.

4. CONCLUSIONS

The dechlorination of CAAs in an aqueous solution has been demonstrated using A-Co-NG as a non-noble metal electrocatalyst, and the dechlorination pathways and mechanisms have been investigated. At pH values of 3.1, 7.2, and 11.2, A-Co-NG/CP completely dechlorinated the CAAs, yielding AA as the final product. TCAA was dechlorinated via a direct mechanism, and its dechlorination pathway was TCAA→DCAA→MCAA→AA. The first ET is the rate-determining step for the dechlorination of TCAA to DCAA, while the dechlorination of DCAA to MCAA follows the synergistic mechanism with the C-Cl bond breaking as the rate-determining step. Owing to its high atomic efficiency and dechlorination activity, A-Co-NG shows great potential for the degradation of chlorinated DBPs in an aqueous phase and, thus, for the removal of these harmful compounds from drinking water.

ACKNOWLEDGMENTS
This research was supported by the National Natural Science Foundation of China (Grant No. 21576238 and 21106133), Natural Science Foundation of Zhejiang Province (Grant No. LY16B060012), Science and Technology Development Foundation of China (Grant No. 20190101A02), Jiangsu Specially-Appointed Professors Program, and Singapore Ministry of Education Academic Research Fund (AcRF; Tier 1: Grant No. RG10/16 and RG111/15 and Tier 2: Grant No. MOE2016-T2-2-004).

References

1. S. H. Zhang, A. J. Guo, N. Wei, R. Zhang and Y. J. Niu, *J. Hazard. Mater.*, 402 (2021) 123452.
2. S. H. Zhang, A. J. Guo, W. X. Zhao, J. L. Gu, R. Zhang and N. Wei, *Environ. Res.*, 177 (2019) 108640.
3. R. B. Smith, M. J. Nieuwenhuijsen, J. Wright, P. Raynor, J. Cocker, K. Jones, M. Kostopoulou-Karadanelli and M. B. Toledano, *Environ. Res.*, 126 (2013) 145.
4. S. Ding, Y. Deng, T. Bond, C. Fang, Z. Cao and W. Chu, *Water Res.*, 160 (2019) 313.
5. Y. Liu, R. Mao, Y. Tong, H. Lan, G. Zhang, H. Liu and J. Qu, *Electrochim. Acta*, 232 (2017) 13.
6. G. Hua, J. Kim and D.A. Reckhow, *Water Res.*, 63 (2014) 285.
7. X. Wang, P. Ning, H. Liu and J. Ma, *Appl. Catal. B Environ.*, 94 (2010) 55.
8. L. L. Lifongo, D. J. Bowden and P. Brimblecombe, *Chemosphere*, 55 (2004) 467.
9. R. Butler, S. Ehrenberg, A. R. Godley, R. Lake, L. Lytton and E. Cartmell, *Sci. Total Environ.*, 366 (2006) 12.
10. J. Nieto-Sandoval, E. Gomez-Herrero, F. El Morabet, M. Munoz, Z. M. de Pedro and J. A. Casas, *Ind. Eng. Chem. Res.*, 59 (2020) 17779.
11. C. Zheng, M. Li, H. Liu and Z. Xu, *Chemosphere*, 239 (2020) 124740.
12. Z. Xia, H. Liu, S. Wang, Z. Meng and N. Ren, *Chem. Eng. J.*, 200 (2012) 214.
13. J. Zhou, K. Wu, W. Wang, Y. Han, Z. Xu, H. Wan, S. Zheng and D. Zhu, *Appl. Catal. B Environ.*, 162 (2015) 85.
14. Y. Cai, X. Long, Y. H. Luo, C. Zhou and B. E. Rittmann, *Water Res.*, 192 (2021) 116841.
15. J. Li, H. Wang, Z. Qi, C. Ma, Z. Zhang, B. Zhao, L. Wang, H. Zhang, Y. Chong, X. Chen, X. Cheng and D. D. Dionysiou, *Appl. Catal. B Environ.*, 268 (2020) 118696.

16. H. Ma, Y. Xu, X. Ding, Q. Liu and C. A. Ma, *Electrochim. Acta*, 210 (2016) 762.
17. Y. Xu, X. Ding, H. Ma, Y. Chu and C. Ma, *Electrochim. Acta*, 151 (2015) 284.
18. Y. H. Xu, H. Zhang, C. P. Chu and C. A. Ma, *J. Electroanal. Chem.*, 664 (2012) 39.
19. B. Liu, X. Hu, Y. Deng, S. Yang and C. Sun, *J. Solid State Electr.*, 16 (2012) 927.
20. X. Zhao, A. Li, R. Mao, H. Liu and J. Qu, *Water Res.*, 51 (2014) 134.
21. A. Li, X. Zhao, Y. Hou, H. Liu, L. Wu and J. Qu, *Appl. Catal. B Environ.*, 111-112 (2012) 628.
22. M. D. Esclapez, I. Tudela, M. I. Díez-García, V. Sáez and P. Bonete, *Appl. Catal. B Environ.*, 166-167 (2015) 66.
23. R. Mao, L. Yan, X. Zhao, R. Djellabi, K. Wang, K. Hu and H. Zhu, *Chem. Eng. J.*, 429 (2022) 132139.
24. Y. P. Li, H. B. Cao and Y. Zhang, *Chemosphere*, 63 (2006) 359.
25. Q. Yao, X. Zhou, S. Xiao, J. Chen, I. A. Abdelhafeez, Z. Yu, H. Chu and Y. Zhang, *Water Res.*, 165 (2019) 114930.
26. S. Almassi, P. R. V. Samonte, Z. Li, W. Xu and B. P. Chaplin, *Environ. Sci. Technol.*, 54 (2020) 1982.
27. L. Z. Huang, S. U. Pedersen, E. T. Bjerglund, P. Lamagni, M. Glasius, H. C. B. Hansen and K. Daasbjerg, *Environ. Sci.* Nano, 4 (2017) 2286.
28. R. Mao, N. Li, H. Lan, X. Zhao, H. Liu, J. Qu and M. Sun, *Environ. Sci. Technol.*, 50 (2016) 3829.
29. G. C. Dubed Bandomo, S. S. Mondal, F. Franco, A. Bucci, V. Martin-Diaconescu, M.A. Ortuño, P. H. van Langevelde, A. Shafir, N. López and J. Lloret-Fillol, *ACS Catal.*, 11 (2021) 7210.
30. L. Jiao, J. Zhu, Y. Zhang, W. Yang, S. Zhou, A. Li, C. Xie, X. Zheng, W. Zhou, S. H. Yu and H. L. Jiang, *J. Am. Chem. Soc.*, 143 (2021) 19417.
31. J. Bok, S. Y. Lee, B. H. Lee, C. Kim, D. L. T. Nguyen, J. W. Kim, E. Jung, C. W. Lee, Y. Jung, H. S. Lee, J. Kim, K. Lee, W. Ko, Y. S. Kim, S. P. Cho, J. S. Yoo, T. Hyeon and Y. J. Hwang, *J. Am. Chem. Soc.*, 143 (2021) 5386.
32. B. H. R. Suryanto, H. L. Du, D. Wang, J. Chen, A. N. Simonov and D. R. MacFarlane, *Nat. Catal.*, 2 (2019) 290.
33. S. Wang, M. Sun, L. Zheng and S. Zhou, *Chem. Catal.*, 1 (2021) 1322.
34. J. Liang, F. Ma, S. Hwang, X. Wang, J. Sokolowski, Q. Li, G. Wu and D. Su, *Joule*, 3 (2019) 956.
35. J. Liu, Z. Gong, C. Allen, W. Ge, H. Gong, J. Liao, J. Liu, K. Huang, M. Yan, R. Liu, G. He, J. Dong, G. Ye and H. Fei, *Chem. Catal.*, 1 (2021) 1291.
36. A. Kumar, V. Q. Bui, J. Lee, L. Wang, A. R. Jadhav, X. Liu, X. Shao, Y. Liu, J. Yu, Y. Hwang, H. T. D. Bui, S. Ajmal, M. G. Kim, S. G. Kim, G. S. Park, Y. Kawazoe and H. Lee, *Nat. Commun.*, 12 (2021) 6766.
37. J. Ding, Y. Ji, Y. Li and G. Hong, *Nano Lett.*, 21 (2021) 9381.
38. Z. Shi, Y. Wang, J. Li, X. Wang, Y. Wang, Y. Li, W. Xu, Z. Jiang, C. Liu and W. Xing, J. Ge, *Joule*, 5 (2021) 2164.
39. T. Wu, S. Sun, J. Song, S. Xi, Y. Du, B. Chen, W. A. Sasangka, H. Liao, C. L. Gan, G. G. Scherer, L. Zeng, H. Wang, H. Li, A. Grimaud and Z. J. Xu, *Nat. Catal.*, 2 (2019) 763.
40. Y. Qiu, J. Zhang, J. Jin, J. Sun, H. Tang, Q. Chen, Z. Zhang, W. Sun, G. Meng, Q. Xu, Y. Zhu, A. Han, L. Gu, D. Wang and Y. Li, *Nat. Commun.*, 12 (2021) 5273.
41. H. Jing, W. Liu, Z. Zhao, J. Zhang, C. Zhu, Y. Shi, D. Wang and Y. Li, *Nano Energy*, 89 (2021) 106365.
42. H. Xu, S. Zhang, J. Geng, G. Wang and H. Zhang, *Inorg. Chem. Front.*, 8 (2021) 2829.
43. A. Wu, J. Yang, B. Xu, X. Y. Wu, Y. Wang, X. Lv, Y. Ma, A. Xu, J. Zheng, Q. Tan, Y. Peng, Z. Qi, H. Qi, J. Li, Y. Wang, J. Harding, X. Tu, A. Wang, J. Yan and X. Li, *Appl. Catal. B Environ.*, 299 (2021) 120667.
44. Y. Xu, Z. Yao, Z. Mao, M. Shi, X. Zhang, F. Cheng, H. B. Yang, H. B. Tao and B. Liu, *Appl. Catal. B Environ.*, 277 (2020) 119057.
45. H. B. Yang, S. F. Hung, S. Liu, K. Yuan, S. Miao, L. Zhang, X. Huang, H. Y. Wang, W. Cai, R.

Chen, J. Gao, X. Yang, W. Chen, Y. Huang, H. M. Chen, C. M. Li, T. Zhang and B. Liu, *Nat. Energy*, 3 (2018) 140.
46. G. Jiang, M. Lan, Z. Zhang, X. Lv, Z. Lou, X. Xu, F. Dong and S. Zhang, *Environ. Sci. Technol.*, 51 (2017) 7599.
47. C. Durante, B. Huang, A. A. Isse and A. Gennaro, *Appl. Catal. B Environ.*, 126 (2012) 355.
48. S. Arnaboldi, A. Gennaro, A. A. Isse and P. R. Mussini, *Electrochim. Acta*, 158 (2015) 427.
49. R. Mao, C. Huang, X. Zhao, M. Ma and J. Qu, *Appl. Catal. B Environ.*, 241 (2019) 120.
50. W. Zhu, T. Huang, M. Qin, M. Li, J. Mack and X. Liang, *J. Electroanal. Chem.*, 774 (2016) 58.
51. W. Y. He, J. M. Fontmorin, P. Hapiot, I. Soutrel, D. Floner, F. Fourcade, A. Amrane and F. Geneste, *Electrochim. Acta*, 207 (2016) 313.
52. N. Hoshi, K. Sasaki, S. Hashimoto and Y. Hori, *J. Electroanal. Chem.*, 568 (2004) 267.
53. Y. P. Li, H. B. Cao and Y. Zhang, *Water Res.*, 41 (2007) 197.
54. I. G. Casella and M. Contursi, *Electrochim. Acta*, 52 (2007) 7028.
55. Z. Mao, L. Liu, H. B. Yang, Y. Zhang, Z. Yao, H. Wu, Y. Huang, Y. Xu and B. Liu, *Electrochim. Acta*, 391 (2021) 138886.
56. A. A. Isse, G. Sandonà, C. Durante and A. Gennaro, *Electrochim. Acta*, 54 (2009) 3235.
57. A. A. Isse, S. Gottardello, C. Durante and A. Gennaro, *Phys. Chem. Chem. Phys.,* 10 (2008) 2409.
58. A. A. Isse, P. R. Mussini and A. Gennaro, *J. Phys. Chem. C*, 113 (2009) 14983.
59. Z. He, L. Zhan, Q. Wang, S. Song, J. Chen, K. Zhu, X. Xu and W. Liu, *Sep. Purif. Technol.*, 80(3) (2011) 526.
60. R. Mao, H. Lan, L. Yan, X. Zhao, H. Liu and J. Qu, *Environ. Sci-Nano*, 5(10) (2018) 2282.